JTTEE5 21:159–168
DOI: 10.1007/s11666-011-9701-6
1059-9630/$19.00 © ASM International

Technique of Formation of an Axisymmetric Heterogeneous Flow During Thermal Spraying of Powder Materials

V.I. Kuz'min, A.A. Mikhal'chenko, O.B. Kovalev, E.V. Kartaev, and N.A. Rudenskaya

(Submitted November 30, 2010; in revised form October 11, 2011)

The paper presents an investigation of a unit of annular injection of powder materials into a thermal plasma flow. The unit is designed for the electric-arc direct-current plasma torch with a sectioned inter-electrode insert up to 100 kW, which was developed earlier. Energy characteristics (thermal efficiency and thermal power of the plasma jet) and spectra of plasma torch current and voltage fluctuations are described. The characteristics of the radial temperature distribution in the plasma jet in the annular and point powder injection cases are compared. A multi-channel spectrometer with a photo-diode array was implemented for the measurements. It is shown that, in contrast to point injection of powder particles, which is carried out across the jet on the nozzle exit, distributed annular injection with gas-dynamic focusing provides a dense axisymmetric heterogeneous flow, in which almost all particles pass through a high-temperature and high-speed area near the plasma jet axis.

Keywords axisymmetric heterogeneous flow, plasma torch with an inter-electrode insert (IEI), refractory material spraying, unit of annular injection of particles

1. Introduction

By now, the conventional technique of injection of a processed powder material into a thermal plasma jet generated by a commercial plasma torch is the point transverse injection (usually at an angle of 90° to the plasma jet axis) through a tube flux duct at the nozzle exit or through an orifice in the nozzle (Ref 1-4). This kind of powder injection significantly disturbs the carrier flow, which enhances the interaction between the plasma jet and the ambient medium, thus, resulting in fast dissipation of energy in the high-temperature area of the jet and in distortion of the radial temperature profile. Because of the resultant non-uniformity of temperature and velocity fields in the plasma jet, the particles in the jet cross sections may have appreciably different thermal and kinetic energy and even may be in different aggregate states. For this reason, the quality of coatings obtained by the plasma spraying method is appreciably deteriorated. Moreover, local point injection has a very low efficiency of plasma jet energy utilization. Normally, it does not exceed 6% (Ref 5).

V.I. Kuz'min, A.A. Mikhal'chenko, O.B. Kovalev, and **E.V. Kartaev**, Khristianovich Institute of Theoretical and Applied Mechanics SB RAS, Novosibirsk, Russia; and **N.A. Rudenskaya**, Scientific and Technological Park of the BNTU "Metolit", Minsk, Belarus. Contact e-mail: kartayev@mail.ru.

The efforts to develop a plasma torch with axial injection of particles through a cathode hole failed because the powder material itself and its vapors affect the

Nomenclature

Latin alphabet

T	Temperature
h	Planck constant
k	Boltzmann constant
c	Light velocity in vacuum
x, y	Coordinates in the Cartesian system of coordinates (mm)
R	Radius of the plasma jet boundary (mm)
$r = (x^2 + y^2)^{1/2}$, $0 \le r \le R$	Radius in the cylindrical system of coordinates (mm)
$Q(T)$	Emissivity of a unit volume (W/m^3)
A_{ik}	Probability of electron transition from the ith to kth level (s^{-1})
$G(T)$	Statistical sum
E	Excitation energy (J)
$I(y)$	Radiation intensity (W/m^2)
F	Oscillator strength
g	Top-level statistical weight
$n(T)$	Concentration of atoms per unit volume (m^{-3})

Greek alphabet

λ	Wavelength of the line under consideration (Å)

arc discharge characteristics and its stability in this case. Deposition of the processed powder on the walls of the plasma torch discharge channel is also a serious obstacle for implementation of this method (Ref 6).

In our opinion, a specially developed unit of annular injection of the powder to be processed shows good prospects for generating an axisymmetric high-temperature heterogeneous flow. In this case, the radially converging axisymmetric flow of particles immediately behind the anode arc spot of the arc discharge can significantly increase the efficiency of plasma jet interaction with the powder, which will improve the quality and rate of material processing. As was shown by theoretical calculations (Ref 7), the annular injection unit allows the efficiency of particle heating and the maximum processing rate to be increased by more than one order of magnitude, as compared with point injection.

Pioneering studies of distributed injection units, wherein powders are injected into the plasma jet through an annular slot, appeared more than 20 years ago. For example, Yermakov et al. (Ref 8) presented an original device model, which contains, in addition to the annular slot for powder injection, an extra annular slot for a focusing gas. However, despite of this fact, we do not know any examples of extensive use of such devices or any standard plasma setups equipped with plasma torches with annular powder injection units. Possible reasons are difficulties with ensuring a stable uniform distribution of the powder over the annular slot, slot plugging with the powder and anode erosion products, or generation of the high-temperature plasma jet with a small opening angle.

The prospects of distributed powder injection through an annular slot and the above-mentioned challenges stimulated the development of an original unit of annular injection and present investigations.

In addition to the technique of powder injection into the plasma jet, arc stabilization in the plasma torch channel also plays an important role in plasma spraying technologies (Ref 9).

Baudry et al. (Ref 10) simulated the arc behavior dynamics in a channel typical for plasma torches with a self-establishing arc length. Fluctuations of the arc length in the anode channel resulting from large- and small-scale shunting were demonstrated to make appreciable contributions to velocity (up to 50%) and temperature (up to 20%) oscillations of the plasma jet at the nozzle exit.

Bisson et al. (Ref 11) studied the influence of voltage fluctuations induced by large- and small-scale shunting of the arc on the parameters (velocity, temperature, and trajectory) of Al_2O_3 and zirconium dioxide single particles stabilized by yttrium dioxide. A plasmatorch with vortex stabilization of the arc was applied. The presence of strong (>20% of the total power) fluctuations within the range of 5-20 kHz and the governing effect of these fluctuations on the particles parameters were observed. Strong harmonics in this spectral range are caused by a high ratio of the typical value of the arc length fluctuation to its average length (1-3 calibers), which is typical for this kind of plasma torches (one caliber is equal to the plasma torch channel diameter).

Nogues et al. (Ref 12) performed a similar analysis of the effect of arc voltage fluctuations in various plasma torches (PTF4, 3MB GE, 3MB G, and Sulzer Metco) with a self-establishing arc length on the thickness of a cold boundary layer in the channel and on the powder velocity and temperature. A series of experiments performed for all types of plasma torches validated the results obtained in Ref 11. Nogues et al. confirmed that the fluctuations of particle velocities and temperatures are related to the thickness of the cold boundary layer in the plasma torch channel, which mainly depends on the arc current and, to a smaller degree, on the plasma-forming gas flow rate.

The purpose of this work is to study the mechanisms of controlling high-temperature heterogeneous flow formation, aimed at improving the effectiveness of the thermal action on powder materials in the thermal plasma jet during plasma spraying. A unit of annular powder injection was developed; it was combined with a d.c. IEI-plasmatorch (Ref 13, 14). Voltage fluctuations induced by arc motion along the channel over the anode are low in this kind of the plasma torch, which is typical for all regimes of its operation.

2. Experimental Investigations

2.1 Annular Injection of the Powder Material

In spite of the fact that the results of Yermakov et al. (Ref 8) were used for the annular injection unit development, our device is based on a novel principle of the uniform powder distribution over the annular slot perimeter. The unit is schematically depicted in Fig. 1. The focusing gas provides the formation of a denser axisymmetric heterogeneous flow.

The heterogeneous flow was visualized by the laser sheet technique (Fig. 2). The laser sheet is a flat beam of radiation 40 mm high, with the thickness corresponding to the Gaussian waist width of ~150 μm. The laser sheet crosses the axisymmetric flow of Al_2O_3 particles, which goes down from the injection unit, over the jet diameter.

The photo of the jet flow in Fig. 3 was produced by the above-mentioned method. It illustrates rigorous focusing of the powder particle trajectories and formation of a dense axisymmetric two-phase flow during cold blowing of the plasma forming, carrier, and focusing gases.

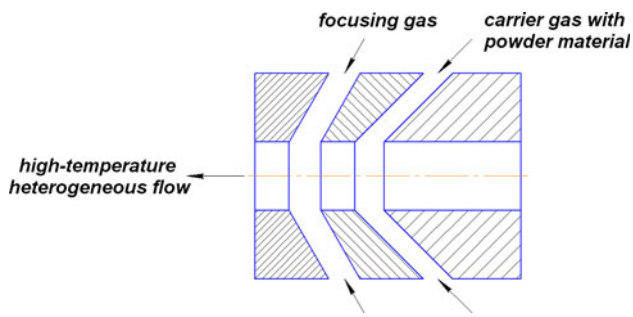

Fig. 1 Layout of the annular unit for powder injection

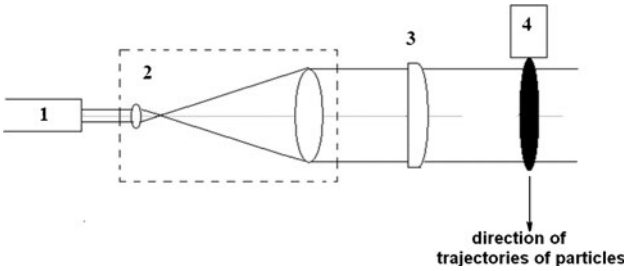

Fig. 2 Visualization of the heterogeneous jet with sprayed particles during cold blowing: 1—laser, 2—collimator, 3—cylindrical lens, 4—plasma torch

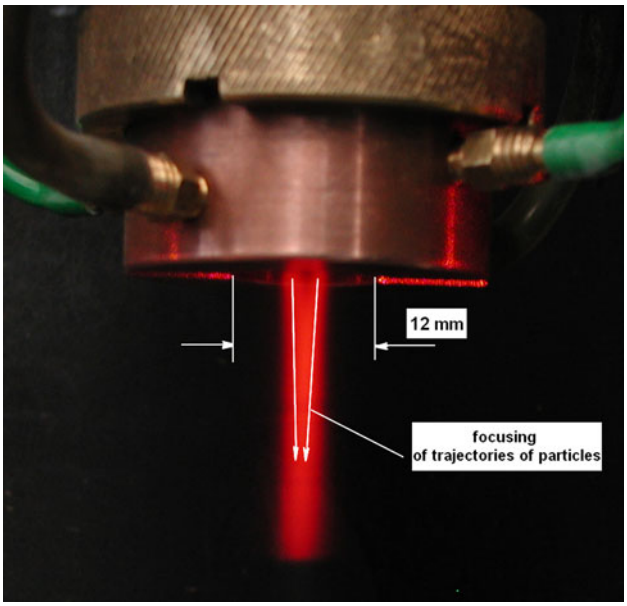

Fig. 3 Laser sheet visualization of the heterogeneous flow during cold blowing

2.2 Design of the d.c. Plasma Torch with the IEI

The plasma torch design is based on a linear model and has an inter-electrode insert (IEI), which provides a much higher working voltage, good axial symmetry of the plasma jet, and minimum fluctuations of the plasma torch parameters as compared with plasma torches having a self-establishing arc length (Ref 14). The IEI-plasma torch is schematically shown in Fig. 4.

The gas-discharge chamber of the plasma torch is a channel expanding from the cathode to the anode; it consists of a series of IEI parts, which are insulated from each other and from the electrodes. The IEI enables not only to fix the arc discharge length in the plasma torch channel, but also to vary the arc length and, hence, the working voltage by varying a number of IEI parts (Ref 14). The electrodes in the plasma torch are a thermochemical cathode (a copper cartridge with a press-fit hafnium insert 2 mm in diameter) and a cylindrical copper anode. All heat-stressed units of the plasma torch are cooled by flowing water.

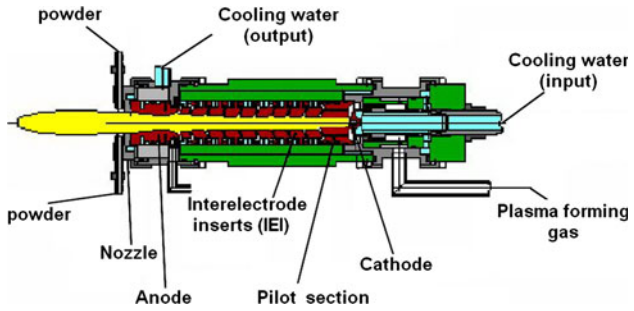

Fig. 4 General layout of the IEI-plasma torch

Either any technically pure gases or air can be used as a plasma-forming, shielding, carrier, and focusing gas. The plasma gas is supplied into the plasma torch channel tangentially from the cathode side with the aid of a vortex ring. The shielding gas is also injected tangentially through the vortex ring into the gap between the last IEI part and anode.

2.3 Energy Characteristics of the Plasma Torch, Operation Modes

Figure 5 shows the volt-ampere characteristics, thermal efficiency, and thermal power of the plasma jet in the plasma torch up to 100 kW (8 IEI parts). The plasma-forming gas was air, and methane was used as the shielding gas.

It should be noted that injection of the shielding gas (methane) practically does not affect the shape of the curves presented in Fig. 5.

The thermal power of the plasma jet was found as the difference between the electric power on the plasma torch arc and the power of heat losses into the plasma torch units (electrodes, nozzle, and channel) as

$$Q_{\text{th}} = U \cdot I - Q_{\text{l}},$$

where U is the plasma torch arc voltage, I is the intensity of the plasma torch arc current, and Q_{l} is the power of heat losses in the plasma torch.

The power of heat losses was determined via calorimetry of heat fluxes into the plasma torch units. For this purpose, the water flow rate and its input/output temperature were measured. The heat losses in the plasma torch units were determined by the formula

$$Q_{\text{l}} = G_{\text{w}} \cdot C_{\text{pw}} \cdot \Delta T_{\text{w}},$$

where G_{w} is the water flow rate, C_{pw} is the water heat capacity, and ΔT_{w} is the difference between the input and output temperatures of water.

The thermal efficiency of the plasma torch was determined as the ratio of the thermal power of the plasma jet to the electric power of the plasma torch arc by the formula

$$\eta_{\text{th}} = \frac{Q_{\text{th}}}{U \cdot I}.$$

The plasma torch is designed to operate in both turbulent and laminar modes (Fig. 6), which permits increasing the plasma jet velocity during metal powder spraying and the

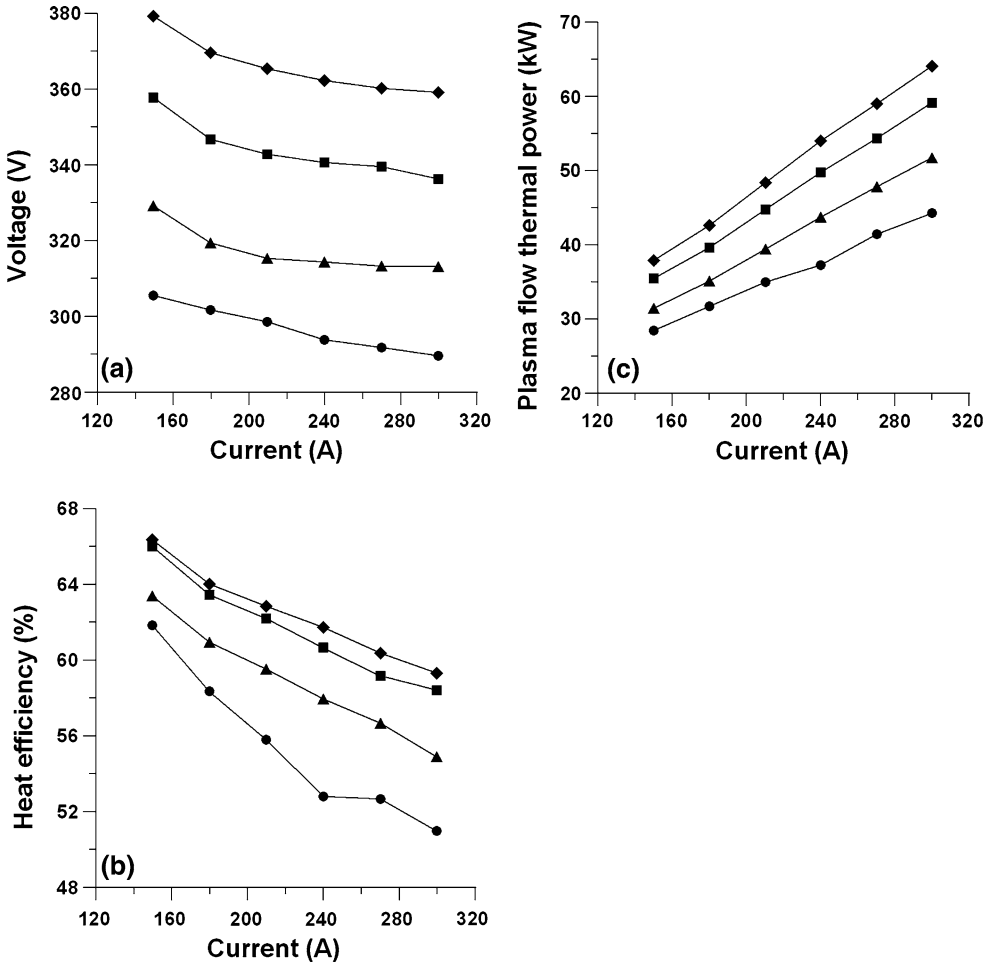

Fig. 5 Volt-ampere characteristics (a), efficiency (b) and thermal power of the plasma jet (c) in the plasma torch (with the IEI, power 70-100 kW, pilot model). The plasma-forming gas is air, the gas for anode protection is methane (9.1 L/min): the data are given for air with the flow rate of 69.2 L/min (circles), 92.3 L/min (triangles), 115.4 L/min (squares), and 138.5 L/min (diamonds)

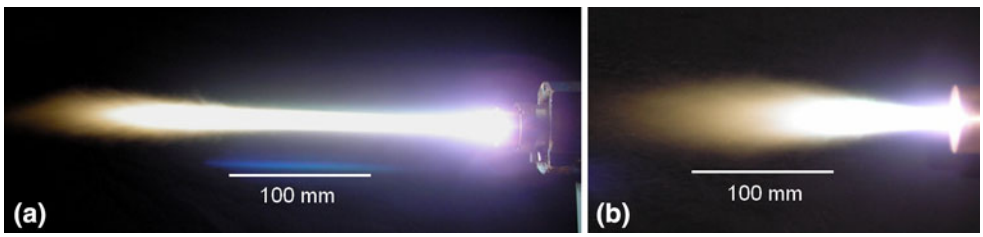

Fig. 6 Modes of the plasma jets flow: (a) laminar jet and (b) turbulent jet

particle residence time in the plasma flow during ceramic powder spraying to the maximum possible extent.

2.4 Spectrum of Current and Voltage Fluctuations in the Plasma Torch

Temporal realizations (up to ~13 ms) were registered by a two-channel high-speed ADC to study the spectral characteristics of the voltage and current fluctuations in the working IEI-plasma torch with a rated power of 100 kW. The time of analog input signals discretization was 400 ns. The signals were recorded within the range of working current variation from 160-200 to 240-300 A with fixed standard flow rates of various plasma gases (air, argon, nitrogen, and carbon dioxide) and with different gas (argon or methane) flow rates for anode protection. The spectra of the current and voltage fluctuations were obtained using the Fast Fourier Transform of the recorded signals.

Figure 7 shows the spectra of the current and voltage fluctuations, and the voltage oscillogram in the time

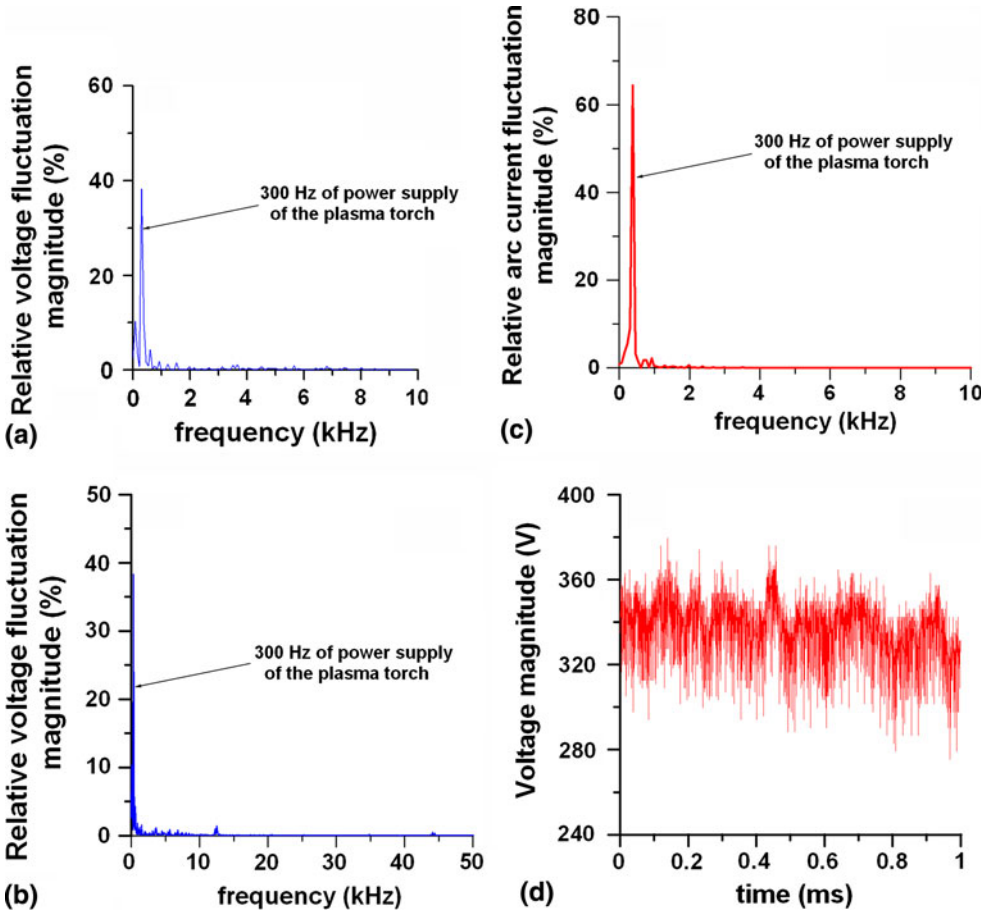

Fig. 7 Spectra of voltage fluctuations (a, b), arc current fluctuations (c), and voltage oscillogram (d) at the plasma-forming gas (nitrogen) flow rate $G_{N_2} = 69.2$ L/min (with no shielding gas), average current of 220 A, and voltage of 335 V

interval of 1 ms for a fixed flow rate of the plasma-forming gas (nitrogen) $G_{N_2} = 69.2$ L/min and current intensity of 220 A. When the working current and the plasma-forming gas flow rate were varied, the pattern of the current and voltage fluctuations was qualitatively unchanged. According to the analysis of the voltage fluctuation spectrum, the high-frequency area of the spectrum (from 20 to 50 kHz) contains almost no harmonics (Fig. 7b), and the greatest part of the spectral power of fluctuations is concentrated in the range below 20 kHz (Fig. 7a). The current spectrum remained constant at any operating conditions and was equal to 300 Hz; this value correlated with the fluctuation spectrum of the combined d.c. power supply (Fig. 7c).

It is known that the spectral area within the range of approximately 1-5 kHz is tied up with the phenomenon of large-scale shunting of the arc along the anode channel. The characteristic times of arc fluctuations near the anode arc spot (small-scale shunting) correspond to the frequency range approximately from 5 to 20 kHz (Ref 14). An analysis of the spectra reveals that, except for the harmonic corresponding to current fluctuations of the plasma torch power supply, the fluctuations caused by the axial arc scanning are low, which is typical for all operation modes of the plasma torch.

2.5 Measurement of the Radial Temperature Distribution in the Plasma Jet with Annular and Point Injection of the Powder

A series of experiments was performed to test the unit of annular injection of particles for ceramic powder spraying.

Air was used as a working gas (plasma-forming, shielding, carrier, and focusing gases).

To study the influence of the carrier and focusing gases on the plasma jet parameters, we measured the plasma temperature distributions at a distance of 5 mm from the plasma torch nozzle exit.

A multi-channel spectrometer with a photodiode array and replaceable concave holographic gratings was utilized for noncontact spectral measurements of plasma flow temperatures. This spectrometer was tested by measuring the temperature distribution of a homogeneous low-temperature plasma flow using atomic spectroscopy (Ref 15). To measure the temperature in the air plasma jet escaping from the d.c. IEI-plasma torch, we chose the atomic copper lines (Cu1) present in the jet because of copper anode erosion.

The spectrometer has the following engineering specifications: average density of grating lines 1200 mm^{-1},

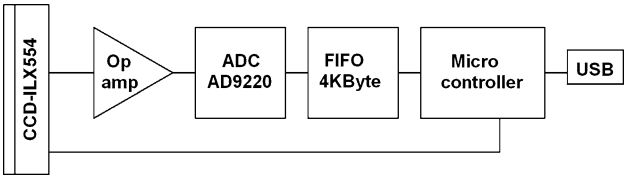

Fig. 8 Flowchart of the device of spectrum detection with a CCD array

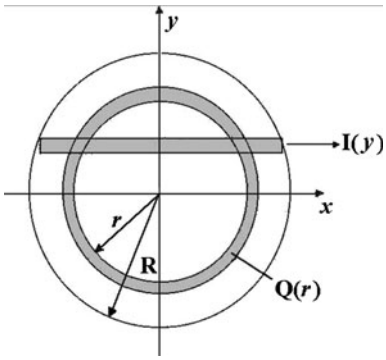

Fig. 9 Plasma jet cross section

spectral range of low-temperature plasma radiation 3000-10,000 Å, and spectral resolution 0.5 Å/pixel for the input slot width of 5 μm.

The structural scheme of the detection device is given in Fig. 8. It includes a CCD array of the ILX554 type (Sony), AD8047 operational amplifier, AD9220 ADC, FIFO buffer memory, and microcontroller. The amplifier provides synchronization of the output CCD signals and ADC. The microcontroller generates control signals for the CCD and scans the CCD signals at the FIFO output. The data are fed into a PC via USB with galvanic insulation. The time of plasma radiation spectrum recording can be varied from 5 ms to 5 s.

The input slot of the spectrometer was 20 μm to have an acceptable level of the signal/noise ratio with the spectral resolution sufficient for Cu1 line detection.

A mercury lamp was used for the wavelength calibration. The absolute calibration was performed with a Si 8-200 tungsten ribbon lamp.

The spectroscopic diagnostics was performed under the assumption that the plasma was in the state of local thermodynamic equilibrium and optically transparent in the spectral ranges chosen for measurements.

The plasma temperature was measured on the basis of the ratio of radiation line intensities. For a given pressure, the radiation density of a unit volume of the plasma in a thermally excited line is related to the temperature as (Ref 16)

$$Q(T) = \frac{c}{4\pi} A_{ik} g \frac{h}{\lambda} \frac{n(T)}{G(T)} \exp\left(-\frac{E}{kT}\right). \quad \text{(Eq 1)}$$

The temperature dependence $Q(T)$ has a maximum at the ''normal'' temperature T_m (Ref 16). In the range of relatively low temperatures $T \ll T_m$, Q rapidly decreases with decreasing temperature.

In an inhomogeneous, optically thin plasma, different plasma layers contribute to the observed intensity; each layer has its own radiation density and thickness. In the case of heterogeneity with axial symmetry, the measured radiation intensity $I(y)$ is related to $Q(r)$ as (Ref 16)

$$I(y) = \int_{-\sqrt{R^2-y^2}}^{\sqrt{R^2-y^2}} Q\left(\sqrt{x^2+y^2}\right) \mathrm{d}x,$$

where $Q(r \geq R) = 0$ and $I(y \geq R) = 0$ (Fig. 9).

In the method of relative intensities, the temperature distribution is found by the formula

$$T(r) = \frac{E_2 - E_1}{k\left(\ln\frac{A_2 g_2 \lambda 1}{A_1 g_1 \lambda_2} + \ln\frac{Q_1(r)}{Q_2(r)}\right)},$$

Here, the subscripts 1 and 2 refer to the first and second lines, respectively.

To find the local values of $Q(r)$, the Abelian inversion method is used (Ref 16).

In this work, the temperature distributions are obtained by the method of relative intensities without involving the Abelian inversion method, by the so-called ''localization method'' (Ref 17). In accordance with this method, under the assumption that the gas flow temperature profile is symmetrical along the x direction and is described by the dependence

$$T(x,y) = \frac{T_0(x=0,y)}{1 + (x/x_0)^2}, \quad \text{(Eq 2)}$$

the maximum temperature $T_0(y)$ along the observation line is found as

$$T(r=y) = \frac{E_2 - E_1}{k \ln\left(\frac{I_1(y)}{I_2(y)} \sqrt{\frac{E_1}{E_2}} \frac{A_2 g_2 \lambda 1}{A_1 g_1 \lambda_2}\right)} = \frac{E_2 - E_1}{k \ln\left(\frac{I_1(y)}{I_2(y)} \sqrt{\frac{E_1}{E_2}} \frac{f_2 g_2 \lambda_1^3}{f_1 g_1 \lambda_2^3}\right)}$$

The ''localization method'' is applicable within the temperature range $T < T_m$, where the spatial behavior of $Q(r)$ depends of the exponential term in Eq 1, which changes drastically with temperature.

Nalivaiko et al. (Ref 15) compared the methods of measurement of the temperature distribution for inhomogeneous objects by means of the Abelian inversion and ''localization method.'' According to their results, the temperature distributions coincide within the instrumental error under the conditions of axial symmetry.

Aside from the methodical error in the case of the Abelian inverse transformation, or approximation accuracy (2) in the case of the ''localization method,'' the temperature measurement error depends on the accuracy of measurement of the spectral line intensities and on the accuracy of data on the spectral line transition probability. Without the methodical error, the error of the temperature measurement can be found by the formula

$$\frac{\Delta T}{T} = \frac{kT}{E_2 - E_1}\left(\frac{\Delta(I_1/I_2)}{I_1/I_2} + \frac{\Delta(g_2 f_2/g_1 f_1)}{g_2 f_2/g_1 f_1}\right). \quad \text{(Eq 3)}$$

The error of the relative values of oscillator forces within one spectrum (second term) can reach 20%. The accuracy of measurement of spectral line intensities with a 10-bit ADC assumed to be 1%, Eq 3 transforms to

$$\frac{\Delta T}{T} = \frac{kT}{E_2 - E_1} * 0.22.$$

The error of temperature measurement within the temperature range from 6000 to 7500 K is, in accordance with Eq 3, $\pm(288 \div 450)$ K.

This method does not require the jet to be symmetric along the scanning direction (y direction, Fig. 9); it was used to study the distorted temperature profile of the high-temperature jet with carrier gas injection. In the case of point powder injection through the tube flux duct, the carrier gas was injected downstream along the OY axis (along the scanning direction).

As mentioned earlier, the measurements of the temperature distribution in the plasma jet were based on the spectral lines of atomic copper Cu1 present in the air jet because of copper electrode (anode) erosion. The spectra were measured for several positions of the observation line. Scanning over the plasma jet diameter was performed by means of mechanical upward motion of the plasma torch with a pitch of 1 mm. The position $y = 0$ corresponds to the extreme top position of the jet, and $y = 14$ mm corresponds to the extreme bottom position where the spectral lines are seen. The spectrum includes the lines of Cu1 at $\lambda = 5105.6$, 5153.2, 5218.2, 5700.2, and 5782.1 Å. The lines pairs $\lambda_1 = 5105.6$ Å, $\lambda_2 = 5153.2$ Å and $\lambda_1 = 5105.6$ Å, $\lambda_3 = 5218.2$ Å were chosen to measure the plasma temperature.

In the case of point powder injection in plasma torches up to 50 kW, ceramic powder spraying is usually performed at moderate flow rates of the plasma-forming gas (up to 46.15 L/min), since it is necessary to increase the residence time for refractory particles with the low thermal conductivity coefficient in the plasma flow for complete melting of the material.

3. Results and Discussion

The results measured in the case of point injection of the carrier gas (without the powder) are presented in Fig. 10(a). During one-sided injection, the carrier gas pushes the high-temperature flow from the injection orifice and distorts its temperature profile. The high-temperature jet axis deviates toward the carrier gas injection point and lies below the plasma torch channel axis. It is evidenced by the shift of the plasma jet temperature profile in Fig. 10(a). When the powder is injected, Fig. 10(b), the plasma torch channel axis, the high-temperature jet axis, and the powder flow axis do not coincide, which results in nonuniformity of particle processing conditions at different trajectories of particle motion.

Figure 11(a) shows the temperature distribution measured in the plasma jet at $z = 5$ mm from the nozzle exit in the case of annular injection. The measurements were

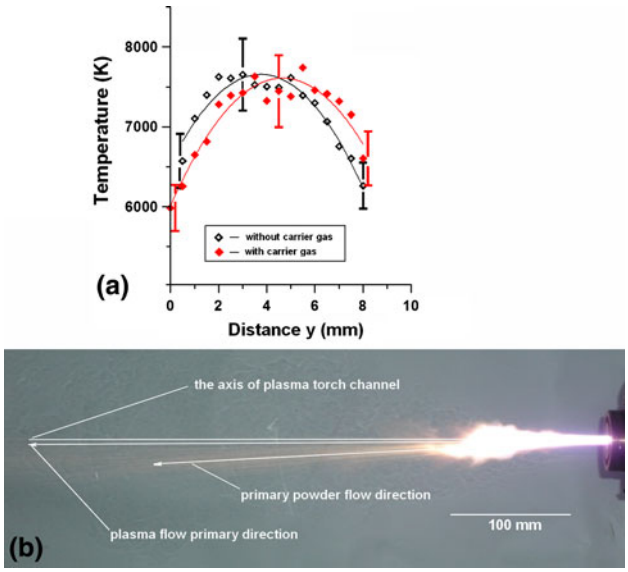

Fig. 10 (a) Temperature distribution in the plasma jet ($I = 200$ A, $U = 205$ V, $G_{\text{plasma(air)}} = 32.3$ L/min, $G_{\text{shield(air)}} = 7.4$ L/min) at the distance $z = 5$ mm from the nozzle exit during one-sided point injection of the carrier gas: without the carrier gas; the flow rate of the carrier gas $G_{\text{carr}} = 2.3$ L/min. (b) Photo of the plasma jet in the case of point injection of the Al_2O_3 powder, particle size 40 μm

performed for the maximum flow rates of the plasma-forming, carrier, and focusing gases, which still ensure sufficiently complete melting of the 40-μm fraction of the Al_2O_3 powder. During axisymmetric injection of the carrier and focusing gases, the plasma jet radiation scanning direction did not matter, since there was no preferential direction of the plasma torch nozzle exit orientation.

As is seen from Fig. 11, injection of the carrier and focusing gases leads to a minor decrease in temperature on the jet periphery only. The central part of the jet remains undisturbed, which vindicates the insignificant depth of penetration of the cold carrier and focusing gases when the annular injection unit is utilized.

The powder was injected in the plasma jet and was collected at the distance of about 1.5 m from the nozzle exit into a water vessel. The effectiveness of particle heating (melting) can be determined by the spheroidization degree. The figure shows the photos of the powder processed under the following conditions: arc current 200 A, arc voltage: (220-270) V, plasma-forming gas flow rate 46.15-92.3 L/min, and flow rate of the Al_2O_3 powder 2.2 kg/h.

The photos of the original Al_2O_3 powder (average size 40 μm) before the processing are shown in Fig. 12, and the particles after the plasma processing (annular and point powder injection are shown in Fig. 13(a)-(h). It is evident that the percentage of unmelted particles increases in the case of point injection (Fig. 13e-h). In addition, it can be noted that unmelted Al_2O_3 particles in the case of annular injection (flow rate 92.3 L/min, Fig. 13c, d) are seen alongside with the fully melted particles; it is caused by the decrease of their residence time in the high-temperature area with increasing plasma-forming gas flow rate.

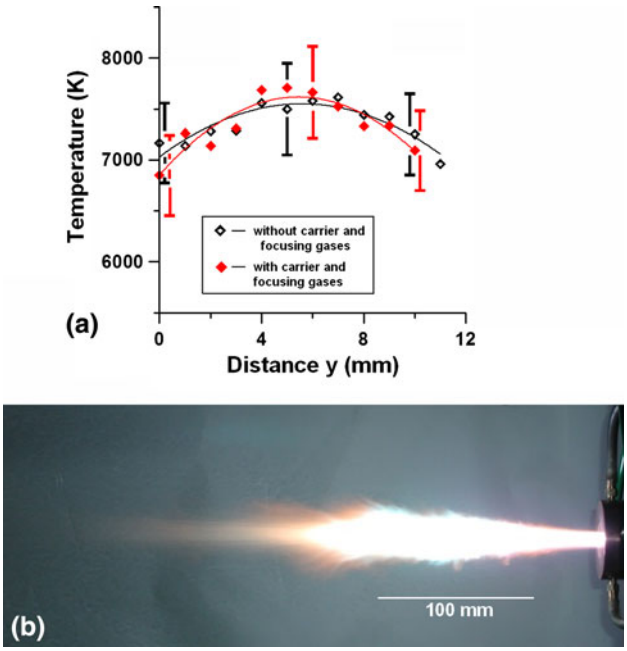

Fig. 11 (a) Temperature distribution in the plasma jet at $z = 5$ mm from the nozzle exit, operating parameters of the plasma torch: $I = 200$ A, $U = 270$ V, $G_{plasma} = 92.3$ L/min; $G_{shield} = 11.5$ L/min; without the carrier and focusing gases; with the carrier and focusing gases with identical flow rates $G_{carr} = G_{foc} = 23.0$ L/min. (b) Photo of the plasma jet in the case of annular powder injection with gas-dynamic focusing

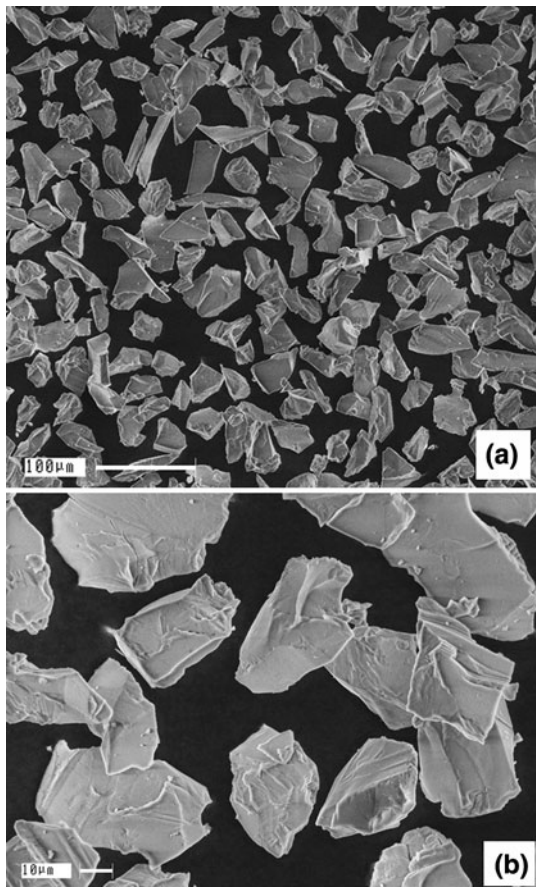

Fig. 12 Photos of the original Al_2O_3 powder with different degrees of magnification (a, b)

These photos clearly illustrate the advantages of annular injection of the powder (almost 100% degree of particle spheroidization).

Thus, annular injection of the powder into the plasma jet provides a higher level of melting of particles at the increased flow rate of the plasma-forming gas (69.2 L/min and more). The increased flow rate results in the increased velocities of the sprayed particles, which influences the quality of the coatings obtained.

The advantages of the above-mentioned methods of powder injection were studied on the basis of a further comparative analysis of the sprayed coating characteristics. Metallographic and structural investigations involved the study of the sample section microstructure, analysis of the interface of the coating and substrate material, microhardness of the coating phases, and coating porosity in general.

The experiments were carried out as follows. To produce a high-quality ceramic coating, a thin sub-layer of the Ni-Al powder with the particle size of 40-100 μm was deposited onto a steel base. The Ni-Al material possesses high adhesion to the base material. In turn, the ceramic base layer also possesses high adhesion to the sub-layer material (the intermetallic component of the Ni-Al system is a standard material used as a sub-layer). Then, the initial powder of aluminum oxide with the particle size of 40 μm was sprayed. The micro-sections are presented in Fig. 14 with 200-fold magnification of the layer-substrate contact area (Fig. 14a) and 500-fold magnification of the basic layer of the coating (Fig. 14b). The following operation conditions were used during ceramic coating spraying: spraying distance 0.1 m, plasma-forming gas (air) flow rate 69.2 L/min, Al_2O_3 powder flow rate 2.2 kg/h, plasma arc current 200 A, and plasma arc voltage 240 V.

A comparative analysis of the deposited layers demonstrated the high-quality coating/basic metal interface (Fig. 14a). The porosity at the interface is low. A metallographic analysis of specific features of the structure of these two-layer coatings shows that the bottom layer is a sub-layer 100-130 μm thick in the form of a white Ni-Al composition (90% of Ni and 10% of Al), whereas the basic top layer 500-550 μm consists of Al_2O_3 and has a gray color. Figure 14(b) clearly shows individual small pores uniformly distributed across the basic layer.

In general, it is established that the coating formed is fairly dense; it has the porosity below 2% and a composite structure. The porosity was determined by the metallographic directed intercept method. Note that the porosity of standard aluminum oxide coatings produced by plasma spraying is 8-15%, as reported in various publications.

4. Conclusion

We propose an effective method of generation of a high-enthalpy two-phase axisymmetric jet flow for plasma

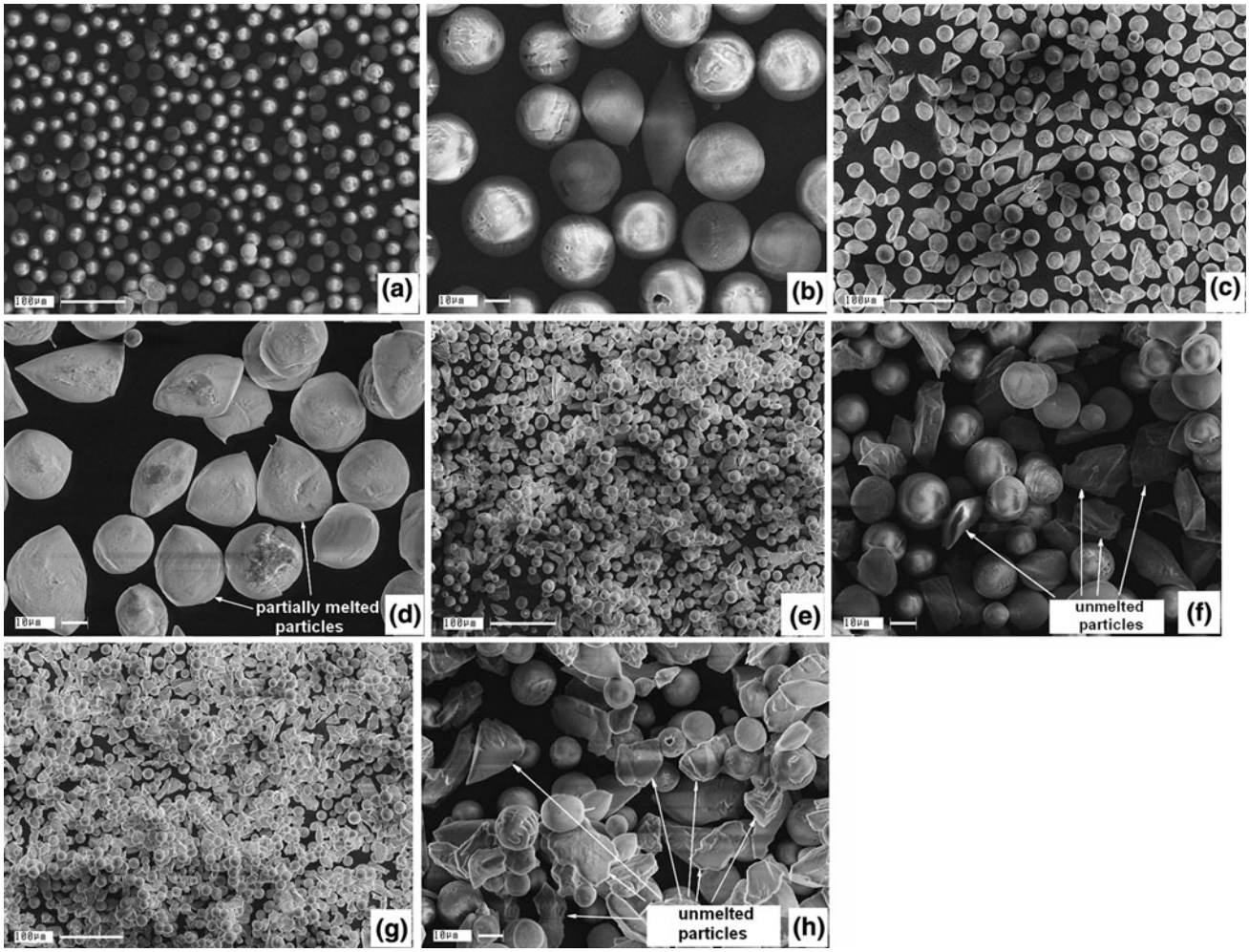

Fig. 13 Comparison of the processing effectiveness during annular injection: (a, b) flow rate 69.2 L/min; (c, d) flow rate 92.3 L/min; during point powder injection: (e, f) flow rate 69.2 L/min; (g, h) flow rate 92.3 L/min

spraying of powder materials. A unit of distributed annular injection of particles, which is combined with a d.c. IEI-plasma torch, was developed for this purpose.

The energy characteristics (thermal efficiency and thermal power of the plasma jet) and the spectra of current and voltage fluctuations are presented. The voltage oscillations induced by the axial motion of the arc along the plasma torch channel are rather low. It is a typical feature, which affects the plasma torch operation mode stability and makes this plasma torch differ from available analogs.

It is demonstrated that the effectiveness of fine material processing in the plasma flow depends on the flow structure in the initial part of the high-temperature dust-laden jet, which, in turn, depends mainly on the plasma torch type, arc burning mode (including the anode spot conditions), as well as the technique of powder injection into the plasma jet.

The radial distributions of temperature in the plasma jet were compared for the cases of point and annular injection. The measurements were carried out with a multi-channel spectrometer equipped with a photodiode array.

When the unit of distributed annular injection is used, all particles of the injected powder pass through the high-temperature and high-speed near-axis area of the plasma jet, which provides a high degree of material melting.

A comparative analysis revealed the advantages of annular powder injection, which slightly disturbs the freely outflowing plasma jet and allows a significant extension of the area of thermal processing of particles, as compared with point injection.

An increased flow rate of the plasma-forming gas provides increased velocities of the powder particles and, under the condition of their complete melting, increases significantly the effectiveness and the quality of coatings. The high quality of coatings is proven by their low porosity. For example, the porosity of the coating of aluminum oxide Al_2O_3, which was produced under optimal conditions (spraying distance 0.1 m, air flow rate 69.2 L/min; powder flow rate 2.2 kg/h, arc current 200 A, and arc voltage 240 V), was below 2%.

The investigations performed present an important aspect of the challenge of developing plasma torches with enhanced controllability of the thermal action on powder

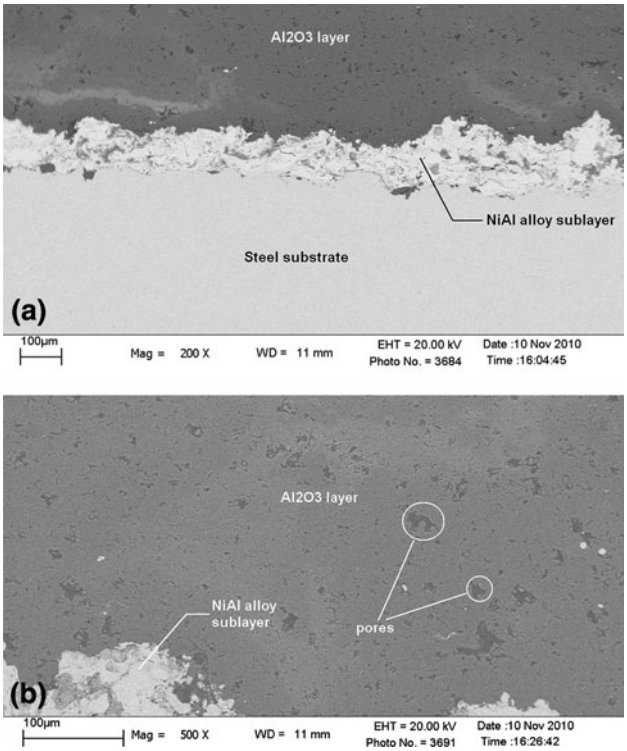

Fig. 14 Microstructure of the two-layer coating: 200-fold magnification of the contact area of the layers (a) and 500-fold magnification of the basic Al_2O_3 coating (b)

materials. In this context, application of the above-described methods of diagnostics of homogeneous and heterogeneous plasma jets is of interest.

References

1. F.E. Beretta and E. Vassallo, Design Criteria for Integrated Injection Systems in a d.c. Plasma Source, *Proceedings of 14th International Symposium on Plasma Chemistry*, 2-6 August 1999 (Prague, Czech Republic), Vol. V, p 2429-2434
2. P. Fauchais and M. Vardelle, Sensors in Spray Processes, *J. Therm. Spray Technol.*, 2010, **19**(4), p 668-694
3. L. An, Y. Gao, and T. Zhang, Effect of Powder Injection Location on Ceramic Coatings Properties When Using Plasma Spray, *J. Therm. Spray Technol.*, 2007, **16**(5-6), p 967-973
4. G. Mauer, R. Vassen, D. Stover, S. Kirner, J.-L. Marques, S. Zimmermann, G. Forster, and J. Schein, Improving Powder Injection in Plasma Spraying by Optical Diagnostics of the Plasma and Particle Characterization, *J. Therm. Spray Technol.*, 2011, **20**(1-2), p 3-11
5. V.S. Klubnikin, ''Electrothermal Plasma Devices and Processes of Powder Materials Spraying,'' Post-Doc Thesis, Kalinin LPI, Leningrad, 1985, 447 pp (in Russian)
6. P. Mohanty, J. Stanisic, J. Stanisic, A. George, and Y. Wang, A Study on Arc Instability Phenomena of an Axial Injection Cathode Plasma Torch, *J. Therm. Spray Technol.*, 2009, **19**(1-2), p 465-475
7. O.P. Solonenko, A.V. Smirnov, and A.L. Sorokin, Interphase Momentum and Heat Exchange in Turbulent Dust-Laden Plasma Jet Under Continuous Radial Powder Injection, *Flow Dynamics: The Second International Conference on Flow Dynamics*, M. Takuyama and S. Maruyama, Ed., 16-18 November 2005, AIP Conference Proceedings (Malville, New York), Vol. 32, 2006, p 375-382
8. S.A. Yermakov, M.V. Karasyov, V.S. Klubnikin, V.M. Maslennikov, N.A. Sosnin, P.A. Topolyanski, and S.Yu. Fyodorov, The Method of Plasma Treatment and the Plasma Torch, Patent WO 90/12123, 1990 (in Russian)
9. J.F. Coudert, M.P. Planche, and P. Fauchais, Characterization of d.c Plasma Torch Voltage Fluctuations, *Plasma. Chem. Plasma Process.*, 1996, **16**(1), p 2115-2275
10. C. Baudry, A. Vardelle, G. Mariaux, C. Delalondre, and E. Meillot, Three-Dimensional and Time-Dependent Model of the Dynamic Behavior of the Arc in a Plasma Spray Torch, *ITSC04 Proceedings*, 2004 (Osaka, Japan), 2004
11. J.F. Bisson, B. Gauthier, and C. Moreau, Effect of Plasma Fluctuations on In-Flight Particle Parameters, *J. Therm. Spray Technol.*, 2003, **12**(1), p 38-43
12. E. Nogues, P. Fauchais, M. Vardelle, and P. Granger, Relation Between the Arc-Root Fluctuations, the Cold Boundary Layer Thickness and the Particle Thermal Treatment, *J. Therm. Spray Technol.*, 2007, **16**(5-6), p 919-926
13. V.I. Kuz'min, A.A. Mikhal'chenko, E.V. Kartaev, and N.A. Rudenskaya, The Annular Injection Unit of Disperse Materials in Thermal Plasma Flow, *24-th International Conference on Surface Modification Technologies (SMT-24)*, Abstracts, 2010 (Dresden, Germany), 2010, p 135-137
14. M.F. Zhukov, I.M. Zasypkin, A.N. Timoshevski, B.I. Mikhailov, and G.A. Desyatkov, *Thermal Plasma Torches. Design, Characteristics, Applications*. Cambridge International Science Publishing, Cambridge, 2007, 596 pp
15. V.I. Nalivaiko, P.A. Chubakov, A.N. Pokrovsky, A.A. Mikhal'chenko, V.I. Kuz'min, and E.V. Kartaev, Small-Size Spectrometer for Emission Analysis of Low-Temperature Plasma Flow, *Thermophys. Aeromech.*, 2007, **14**(2), p 247-256
16. W. Lochte-Holtgreven, Ed., *Plasma Diagnostics*. North-Holland Publishing Company, Amsterdam, 1968
17. P. Frugier, C. Girold, S. Megy, C. Vandensteendam, E.A. Ershov-Pavlov, and J.-M. Baronnet, OES Use and Vaporization Modeling for Fly-Ash Plasma Vitrification, *Plasma. Chem. Plasma Process.*, 2000, **20**(1), p 65-86